Transportation Research Part D 154 (2026) 105270

Contents lists available at ScienceDirect

Transportation Research Part D

journal homepage: www.elsevier.com/locate/trd

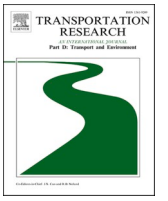

Revealing uncertainties of on-road emissions in a mountainous city using multi-source data

Zeyu Zhang [a], Qiuzi Chen [b], Weizhen Lin [a], Ran Tu [c], Wenyu Wang [a], Xiaotong Zhang [a], An Wang [a,*]

[a] Department of Civil and Environmental Engineering, Hong Kong Polytechnic University, Hong Kong, China
[b] School of Architecture, Civil and Environmental Engineering, École Polytechnique Fédérale de Lausanne (EPFL), Switzerland
[c] North Central Texas Council of Governments

ARTICLE INFO

Keywords:
Multi-source data
City-scale emission modeling
Road grade
Computer vision
Vehicle electrification

ABSTRACT

Robust on-road traffic emission modeling supports carbon reduction, pollution control, and energy transition planning. While road grade surely affects individual vehicle emissions, its city-scale impact remains underexplored. This study integrates multi-source data from Hong Kong (HK)—dynamic fleet composition, spatially resolved traffic simulation, and geographic information—to capture spatiotemporal emission patterns. A grade-included link-level emission model is developed based on the local regulatory grade-invariant model and validated by extensive on-road plume-chasing experiments. Results show that incorporating road grade increases citywide carbon and air pollutants by 10–30% and substantially alters their spatial distribution, with over 50% of road segments deviating by more than 10% from grade-invariant estimates. Road grade's emission effects cannot be fully offset in mountainous cities like HK, while the effects are both local and regional. Leveraging the high-resolution emission model, we further find an about several-year delay in achieving HK's 2035 carbon reduction goal for on-road transportation.

1. Introduction

Robust on-road emission modeling is valuable for urban air pollution management and low-carbon transportation planning at the vehicle, road, and city scales or larger spatial scales. Among myriad methods, the bottom-up modeling approach balances spatio-temporal resolutions, study scopes, and computational complexity. At the city scale, the traditional approach combines static travel surveys or traffic assignment with link-level, average-speed emission factors to capture spatiotemporal traffic dynamics (Yang et al., 2019; Zhang et al., 2016), already demonstrating good performance. Increasingly, emerging multi-source traffic and emission data have significantly advanced city-scale bottom-up emission modeling. Machine learning and AI have enhanced the utilization of multi-source data, further improving the spatio-temporal resolution of bottom-up emission modelling (Li et al., 2024; Wen et al., 2020; Zhang et al., 2018). These methods integrate various data types such as traffic flow data, geographic information, and environmental data, enabling more accurate emission estimates at both link-level and hour-level by capturing dynamic changes in traffic and environmental conditions, and reducing uncertainty in emission estimation (Wang et al., 2023a; Wen et al., 2022, 2024).

Multiple factors influence uncertainties in bottom-up emission modeling, with impacts varying due to each city's distinct fleet composition, road network, and traffic characteristics (Fu and Wu, 2025; Lang et al., 2025; Liu et al., 2018; Wen et al., 2023). This

* Corresponding author.

https://doi.org/10.1016/j.trd.2026.105270
Received 20 October 2025; Received in revised form 25 January 2026; Accepted 8 February 2026
Available online 17 February 2026

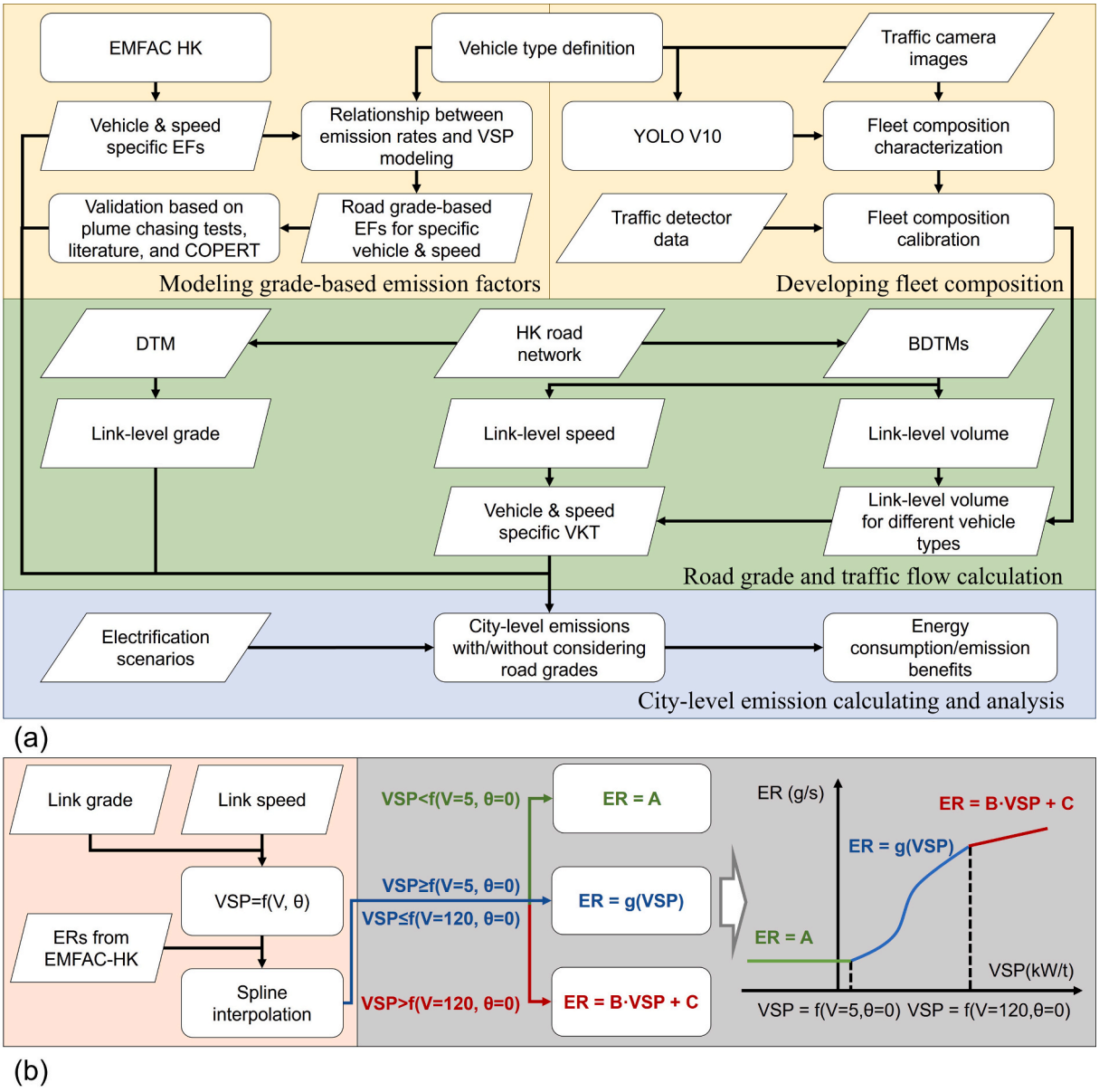

Fig. 1. (a) Research framework with four modules: (1) modeling road grade-based emission factors, (2) developing fleet composition via computer vision, (3) calculating link-level road grade and traffic flow, and (4) estimating city-scale emissions, including the effects of road grade and different electrification scenarios. VSP refers to Vehicle Specific Power; DTM refers to Digital Terrain Model; BDTMs refers to the 2019 Base District Traffic Models; and VKT represents Vehicle Kilometers Travelled. (b) Framework of modeling the relationship between VSP and emission rates. θ is road grade, $VSP = f(V, \theta)$ is the empirical function for calculating VSP, $g(VSP)$is the spline interpolation function describing the relationship between VSP and emission rates (ER), A is $g(VSP)$ at $VSP = f(V = 5, \theta = 0)$, B is the slope of $g(VSP)$ at $VSP = f(V = 120, \theta = 0)$.

highlights the need for city-specific modeling frameworks. Our study identifies two outstanding uncertainty sources in current city-scale bottom-up emission models. First, static vehicle registration data is used to estimate fleet average emission factors, which not necessarily represent the actual on-road fleet composition. Recent literature has explored the use of computer vision for fleet composition estimation (Morris et al., 2012). Deep learning models have demonstrated exceptional performance in vehicle detection across various traffic scenarios (Ma and Xue, 2024). Two-stage vehicle detection algorithms have achieved strong performance under diverse traffic and weather conditions (Kumar et al., 2025; Ojha et al., 2021; Satyanarayana et al., 2022). To maximize detection speed, single-stage models represented by YOLO have been increasingly applied to vehicle recognition (Bhujbal and Mane, 2020; Kumar et al., 2022; Nekkanti and Rao, 2023; Yang et al., 2024). Wang et al., (2020a,b) employed YOLO for vehicle classification to support emission estimation and hotspot analysis. These studies show that computer vision enables link-level fleet composition development and thereby traffic flow estimation.

Second, while road grade is recognized as an important factor affecting vehicle emissions, its impacts are often simplified in city-scale emission models, assuming that uphill and downhill emissions compensate (Liu et al., 2023, 2022). Some studies seem to support this assumption, such as, Frey et al., (2008) found that road grade's impact on emissions was smaller at the route level than at the link level. Meanwhile, regulatory emission models often overlook or cannot explicitly incorporate road grade effects, including COPERT, EMFAC, and HK's EMFAC-HK (CARB, 2021; HKEPD, 2021a; Ntziachristos et al., 2009). Nonetheless, this assumption has been challenged: downhill segments may reduce emissions, but their effects are inconsistent (Wyatt et al., 2014; Zachiotis and Giakoumis, 2020). A HK local study found that combined uphill and downhill emissions were higher than those on flat segments (Papadopoulos et al., 2020). This highlights the necessity of exploring road grade's effects in city-scale emission modeling, especially in mountainous cities like HK.

Our study develops a bottom-up framework using multi-source data from HK to minimize uncertainties from fleet composition and road grade in city-scale emission accounting. We first leverage publicly available traffic camera and counter network in HK and a computer vision-based vehicle classification algorithm to estimate city-wide on-road fleet composition. Road grade is obtained by overlaying the HK road network with digital elevation maps. Revising HK's regulatory emission model, we develop a link-level (road segment by segment) emission inventory of greenhouse gases and multiple on-road air pollutants with validation from real-world plume-chasing experiments. This study contributes to existing literature in two main aspects. First, we provide a policy-relevant methodological refinement for city-scale traffic emission inventories by coupling multi-source urban data, enabling dynamic, link-level fleet composition representation and independent validation under real-world conditions, and explicitly quantifying uncertainties associated with road grades, emission factors, fleet composition and traffic flow. Second, we explicitly quantify the impact of road grade on city-scale road traffic emission estimation, thereby revealing the potential bias introduced when topographic effects are neglected in mountainous cities. In particular, widely used regulatory emission models, including MOVES, COPERT, EMFAC, and the locally adopted EMFAC-HK, do not fully account for road grade in city-scale emission inventories. To enable localized emission modeling while remaining consistent with locally adopted regulatory emission factors, this study develops an approach to correct EMFAC-HK emission factors for road-grade effects, providing a practical reference for incorporating topographic effects into city-scale emission models. This is crucial for academics and practitioners reconsidering transportation energy transition and urban air pollution control policies, given gaps in emission estimation.

2. Materials and methods

The overall framework is illustrated in Fig. 1 (a). First, road grade-based emission factors (EFs) are established. Vehicle specific power (VSP) values are calculated based on vehicle classification results, and EFs are extracted and integrated from EMFAC-HK to construct the relationship between VSP and emission rates, yielding EFs that account for road grade. These grade-included EFs are validated through plume chasing tests, literature, and the official European emission inventory model COPERT. Next, link-level fleet composition is constructed: Camera images are labeled to train a YOLO model for preliminary fleet estimation, then refined with traffic detector data and spatially interpolated using inverse distance weighting. Subsequently, link-level road grades are derived from Digital Terrain Model (DTM) data, and vehicle kilometers traveled (VKT) by vehicle class are obtained from the 2019 Base District Traffic Models (BDTMs) and fleet composition. Finally, using road grade-based EFs, road grades, and VKT, link-level emissions are estimated and aggregated to city scale. Various electrification scenarios are further evaluated to analyze potential energy savings and emission reduction benefits.

Beyond the procedural workflow, the proposed framework offers several methodological advantages for city-scale traffic emission modeling. First, by using VSP as an intermediate parameter, we establish grade-included EFs for specific vehicle classes and speeds, which are directly anchored to the locally adopted emission model and independently validated using real-world plume-chasing experiments and external references. This design provides a practical methodological extension to existing regulatory emission models. Second, the fleet composition construction based on roadside camera data and computer vision enables a dynamic, link-level representation of on-road vehicle fleets. Compared with conventional approaches relying on static vehicle registration data, this data-driven strategy substantially reduces uncertainty in city-scale emission modeling associated with spatial and temporal heterogeneity of fleet composition. Third, the framework is built entirely on open and publicly available data sources, forming a transferable paradigm for high-resolution urban emission modeling. The modular design allows the approach to be adapted to other cities with similar data availability, particularly where detailed fleet dynamics and road grade effects are relevant.

2.1. Road grade calculation

The digital elevation data is based on the Digital Terrain Model (DTM) released by the Lands Department of HK (HKLD, 2019) (Table S1, ESI section C1). Road grade is calculated by integrating DTM with the HK road network via latitude-longitude matching (Fig. S1, ESI section C1), providing elevation for each point. Roads are divided into links as follows: First, road segments longer than 100 m are split into multiple 100-meter links. Remaining segments shorter than 100 m are retained as individual short links, whose grades are calculated using the elevations of their endpoints. Second, each 100-meter link is broken into three random-length parts, where each part should be at least 20 m long, and the link grade is computed as the average of the grades of the three parts. Since tunnel elevations cannot be reliably obtained and tunnels account for less than 0.8% of VKT, their grades are set to zero. To validate our calculation method, the same procedure is applied to the HK 3D Pedestrian Network Map (HKLD, 2022), which provides sidewalk grade data, allowing a comparison between calculated and embedded grades.

2.2. Link-level traffic flow development

Link-level traffic flow data are derived from the 2019 Base District Traffic Models (BDTMs), published by the Transport Department of HK (HKTD, 2021). Constructed using local travel surveys and calibrated with traffic counts, BDTMs simulate the physical road network and traffic conditions during weekday morning and evening peak periods, providing information including coordinates, traffic demand, equivalent traffic volume, and hourly average speed for different routes. The model demonstrates strong calibration accuracy, with over 96% of links achieving a GEH error (Friedrich et al., 2019) of 5 or less, at least 85% of links differing by less than 10% from observed flows, and more than 97% within 20%. GEH error refers to the Geoffrey E. Havers (GEH) statistic, which is an empirical formula to evaluate the goodness-of-fit between observed and modeled traffic volumes. It is worth noting that BDTMs use simplified street network for modeling. To get link-level traffic flow, we geo-reference BDTMs traffic flow data to the real-world HK road network, given the proximity of endpoints and center points as well as traffic directions. Still, we miss about 30% of road links after spatial matching, where we use the inverse distance weighting method to interpolate traffic flow data for these links.

2.3. Fleet composition characterization

Real-world fleet composition is rarely used in city-scale emission modeling due to limited categorized traffic flow data. Our study characterizes the city-wide fleet composition using a unique dataset, taking advantage of the good coverage of traffic cameras and counters in HK. Considering that some vehicle classes have similar visual appearances, we merge certain types to improve image recognition robustness. The merging process and uncertainty are tested in the SI, Section C2 and C10. We identify eight vehicle classes: passenger cars (PC), taxis (TAXI), motorcycles (MC), light-duty buses (LDB), heavy-duty buses (HDB), double-decker buses (FBDD), light-duty goods vehicles (LGV), and heavy-duty goods vehicles (HGV) (SI, section C2). The merging principles are: (1) PC, TAXI, FBDD, and MC are not merged due to their visually distinctive characteristics; (2) HGV, LGV, LDB, and HDB are merged into broader categories by grouping their weight-based subclasses defined in EMFAC-HK.

We use the open-sourced roadside surveillance snapshot images to derive spatial-temporally resolved on-road fleet composition from HK Transport Department. The framework is structured into three key steps (Fig. S5, ESI section C2): (i) developing a Hong Kong-specific vehicle detection and classification model based on computer vision and human-annotated vehicle classes; (ii) calibrating the computer vision-derived fleet composition using paired camera-detector observations; and (iii) applying the trained classification and calibrated fleet composition models to the full image dataset to generate link-level, temporally and spatially resolved classified traffic flows for the entire Hong Kong road network.

2.4. Impact of road grade on the emission factor

Emission FACtor (EMFAC) model, developed by the California Air Resources Board, is an average speed-based emission model for assessing on-road emissions and regulatory and air quality planning (CARB, 2021). HK Environmental Protection Department adapted the model with locally measured emissions and vehicle activity data to develop its HK version, EMFAC-HK for regulatory and decision-making purposes. Same as the original EMFAC, EMFAC-HK has no consideration of road grade's emission effects, ignoring the mountainous landscape locally. To address this, we use the Vehicle Specific Power (VSP) as an intermediary parameter to quantify grade effects on EFs at different speeds. VSP, the power output per unit mass of engine traction (kW/t), is calculated based on fundamental vehicle kinetic laws (Equation (1) (Jimenez-Palacios, 1998)) and is widely applied in fuel consumption and emission calculations (Mera et al., 2022; Wang et al., 2022). For ease of calculation, we use the empirical functions and coefficients (Eq. S1, Table S5, ESI section C3) from MOVES to calculate VSP for different vehicle classes at the link level (U.S. EPA, 2023). The key parameters include speed-dependent terms that approximate rolling resistance (A), mechanical/rotational losses (B), and aerodynamic drag (C), and a grade-related term that represents gravitational power demand (via gsinθ). In MOVES, the parameters used for VSP calculation are determined by vehicle class. For each of the eight HK vehicle classes, we therefore adopt the corresponding MOVES VSP parameters (SI section C3). While acceleration/deceleration has apparent emission effects on individual vehicle drive cycles (Suarez et al., 2022), this term is simplified in our emission model for mainly two reasons. First, to better integrate with the local regulatory model (EMFAC-HK), we use the same baseline average speed-based EFs and modeling approach, where the emission effects of acceleration/deceleration are not considered. Other than EMFAC-HK, city-scale emission modeling using other major regulatory models COPERT (Tier 3) and MOVES (county/national scale) also does not explicitly express this term (Lejri and Leclercq, 2020; Li et al., 2020). Nonetheless, acceleration/deceleration's effects are inexplicitly inherited from emission test cycles when developing average speed-based EFs. Second, previous literature (Wang et al., 2022, 2020a) has demonstrated that acceleration/deceleration has limited impacts on city-scale emission totals, regardless of local drive cycles. Therefore, we adopt the traditional average speed-based emission modeling method to match the modeling granularity with the regulatory models, which also improves computational efficiency and reduces data requirements.

$$VSP = \frac{\frac{d}{dt}(KE + PE) + F_{rolling} \bullet v + F_{Aerodynamic} \bullet v}{M} \tag{1}$$

Where, $\frac{d}{dt}(KE + PE)$ is the power consumed by changes in the vehicle's kinetic energy (KE) and potential energy (PE), in kW. $F_{rolling} \bullet v$ is the power to overcome rolling resistance, in kW. $F_{Aerodynamic} \bullet v$ is the power consumed to overcome air resistance, in kW. M is the source mass in tons. v is speed in m/s.

To quantify the effect of road grade on speed-specific emissions, this study models the relationship between VSP and emission rates (ERs, with units in g/s), rather than directly with EFs. This approach is adopted as EFs are inherently expressed using a function of the ERs and VSP; therefore, VSP alone cannot accurately capture variations in EFs, while a direct VSP-ER relationship can be mathematically modeled (U.S. EPA, 2023). Under constant environmental conditions (e.g., temperature, relative humidity, etc.), ERs are considered dependent solely on the vehicle's engine power output. The developed function characterizes this relationship. When speed remains constant, changes in grade cause variations in VSP, thereby affecting ERs.

For each pollutant of each vehicle class, the quantification procedure is illustrated in Fig. 1(b).

1) EFs from 5–120 km/h at 5 km/h intervals, are obtained from EMFAC-HK. To maintain consistency with the traffic flow data, which represents a typical weekday in 2019, the EFs are selected under 2019 weather conditions, assuming an average temperature of 25°C and an average relative humidity of 80%. Since EMFAC-HK does not account for road grade, these EFs are treated as baseline values (grade = 0). Without considering road grade, VSP is a function solely dependent on the average link speed (acceleration = 0).

2) For each speed, the corresponding VSP is calculated, and EFs are converted to ERs using Equation (2). Spline interpolation is applied to the resulting ER-VSP curve for $f(V=5, \theta=0)$ <=VSP <=$f(V=120, \theta=0)$, establishing a continuous mathematical model.

$$ER = \frac{EF \bullet V}{3600} \tag{2}$$

Where, ER is the emission rate, measured in g/s. EF is the emission factor, measured in g/km. V is the speed, measured in km/h.

3) For VSP < $f(V=5, \theta=0)$, ERs remain constant (U.S. EPA, 2023), where we take the interpolated ERs at $f(V=5, \theta=0)$ as a flat value to define the ER-VSP relationship. Physically, the engine is on but does not output power in this VSP range to maintain the vehicle's original kinetic condition.

4) For VSP > $f(V=120, \theta=0)$, where ERs' increase hits an elbow point, a linear function is fitted (U.S. EPA, 2023). The slope is determined by the derivative of the spline curve at $V=120, \theta=0$.

Based on this method, the ER-VSP relationship for a specific vehicle class is formulated as Equation (3):

$$ER = \begin{cases} A, vsp < f(V=5, \theta=0) \\ g(vsp), f(V=5) \le vsp \le f(V=120, \theta=0) \\ B \bullet vsp + C, vsp > f(V=120, \theta=0) \end{cases} \tag{3}$$

where g is the spline interpolation function, and A, B, and C are defined by Equation (4), (5), and (6).

$$A = g(f(V=5, \theta=0)) \tag{4}$$

$$B = g'(f(V=120, \theta=0)) \tag{5}$$

$$C = g(f(V=120, \theta=0)) - B \bullet f(V=120, \theta=0) \tag{6}$$

2.5. Validation of grade-included emission factors

To verify the validity of the proposed grade-included EF model, we conduct validation based on field measurements and literature references. We conducted on-road plume chasing measurements in HK between April 9 and June 26, 2025. This method enables the large-scale collection of real-world vehicle emissions (Wang et al., 2023b; Xiang et al., 2023, 2025). We collect extensive exhaust plume concentration data from HGV, which are then processed to calculate both fuel-based and distance-based EFs. This allowed us to analyze how real-world HGV EFs vary across different speeds and road grades, thereby providing a robust validation of the grade-included EF model proposed in this study. The validation based on literature is conducted using both a literature (He et al., 2022) and COPERT model (Ntziachristos et al., 2009). We also obtain EFs for different vehicle classes under various road conditions from both the literature and the COPERT model. Further methodological details are provided in SI, section C9.

Relative ratios are calculated by normalizing EFs against the value at 0 grade, which isolates the relative effects of road grade on EFs. An agreement metric, $R^2_{\text{model vs test}}$ is defined as the coefficient of determination between the relative ratios calculated from our model and the fitted exponential curve based on the plume chasing tests or literature and COPERT (SI, section C9).

2.6. City-scale emissions calculation under various electrification scenarios

The bottom-up emission model operates as follows: For each road link in the network, we calculate its grade, traffic flow, and fleet composition. Using these inputs, we derive the VKT and average speed for each vehicle class on that link. The emissions for each link are then computed by multiplying the VKT of each vehicle class by the corresponding speed-specific grade-included EFs. The emissions from all links are aggregated to obtain the total network-level emissions. The emission calculation for the entire network can be expressed as:

$$Emissions_{city} = \sum_{i=1}^{N} \sum_{p=1}^{8} f\left(VKT_{i,p}, EF_p(grade_i, speed_i)\right) \tag{7}$$

Where, i represents each road link, p represents each vehicle class, $VKT_{i,p}$ is the VKT for vehicle class p on link i, EF_p is the EF for vehicle

class p at $grade_i$ and $speed_i$, $grade_i$ is the road grade on link i, $speed_i$ is the average speed of link i.

We further estimate city-scale CO_2 emissions from PC under different CO_2 emissions intensity of electricity sold (EIES) and electric PC (EV) penetration rate scenarios, focusing on on-road emissions. For gasoline PC, CO_2 emissions are calculated using the EFs developed in this study. For EVs, CO_2 emissions are estimated based on EIES and vehicle energy consumption. Road grade impacts on EV CO_2 emissions are quantified through road grade effects on energy consumption, also using VSP as an intermediary. EV energy consumption rates and factors by road grade are shown in SI, section C4. Negative energy consumption rates occur when VSP is below zero, representing net energy recovery through regenerative braking under downhill or decelerating conditions. As the analysis is conducted at the city scale using average speeds, this formulation represents average operating conditions and does not explicitly resolve transient braking events.

City-scale CO_2 emissions of PC in 2005, and from 2020 to 2050 are calculated using Equation (8)

$$Emissions = \sum_i [Emission_i \bullet (1-\alpha) + Energy_i \bullet \alpha \bullet EIES] \bullet \frac{VKT_y}{VKT_{2019}} \tag{8}$$

Where, $Emission_i$ is the CO_2 emissions of gasoline PC on link i in 2019; $Energy_i$ is the energy consumption of EV on link i in 2019; α is the penetration rate, from 0% to 100%; $EIES$ is the CO_2 emissions intensity of electricity sold, from 0.5 kg/kWh to 0 kg/kWh; VKT_y is the city-scale VKT of PC in year y; VKT_{2019} is the city-scale VKT of PC in 2019.

The VKT of PC in 2005, 2019, and 2020 to 2050 is obtained from EMFAC-HK. Emissions and EV energy consumption of each link in 2019 are calculated using the same bottom-up approach. EV penetration rate is set to 0 in 2005, and half of that year's CO_2 emission is set as the 2035 emission reduction target (HKEPD, 2021b). Annual EIES and EV penetration rates are obtained from a World Resources Institute (WRI) report (WRI, 2022), which develops long-term decarbonization pathways for HK using an integrated scenario framework (the Hong Kong Energy Policy Simulator) with internally consistent assumptions on technology adoption and policy implementation. For EIES, we adopt the projected values representing the most ambitious fossil-free scenario toward carbon neutrality by 2050, with a power mix of 60% imported nuclear, 30% hydrogen-based, and 10% local renewables. For the EV penetration rate, we follow the "current policy scenario", in which the sale of internal combustion engine vehicles will be banned by 2035. Given HK's already high public transport mode share (>90%), there is limited scope for further TDM-driven mode shifts (WRI, 2022). Therefore, the overall development trend of PCs is not expected to change substantially. This combination—low-carbon electricity, widespread EV adoption, and rising car ownership—is hereafter referred to as the current policy projection.

2.7. Uncertainty analysis

To quantitatively assess how uncertainties in key inputs propagate through the emission estimation framework, we employ a Monte Carlo simulation approach. Deterministic results obtained from the original input data are treated as baseline estimates, representing emission outcomes without stochastic perturbations. In the Monte Carlo simulations, five major sources of uncertainty are considered: road grade derived from DTM data, EFs associated with vehicle class aggregation (merged classes including LDB, HDB, LGV, and HGV), computer vision-based fleet composition estimation, fleet composition interpolation to the full link-level road network, and traffic flow derived from the BDTMs. The overall uncertainty propagation pathway is schematically illustrated in Fig. S39 ESI section C12.

In the Monte Carlo simulations, road grade uncertainty is represented by perturbing link-level road grade using a zero-mean normal distribution, with the perturbation magnitude informed by the reported DTM vertical accuracy (±5 m at the 90% confidence level) and the corresponding link length. Vehicle class aggregation uncertainty in EFs is represented by probabilistically sampling EFs from the original constituent vehicle subtypes within each merged category, using their VKT shares as sampling probabilities. Uncertainty in computer vision–based fleet composition is represented by applying additive zero-mean normal perturbations to calibrated vehicle class proportions, with the perturbation magnitude informed by empirical calibration mean absolute error obtained from camera–detector validation. Additional uncertainty arising from fleet composition interpolation is represented by applying further additive zero-mean normal perturbations to link-level fleet shares, with the perturbation magnitude informed by the mean absolute error observed in the interpolation validation. Traffic flow uncertainty from BDTMs is represented by applying a multiplicative normal perturbation factor with unit mean to link-level flows, with the standard deviation set such that ± 10% corresponds to an 85% confidence interval.

Emissions are recalculated for each Monte Carlo realization. For the experiment mode jointly perturbing all uncertainty sources, uncertainty ranges are summarized using mean values and 95% confidence intervals to characterize the overall uncertainty of the proposed emission estimation framework. To disentangle the contributions of different uncertainty sources, five additional Monte Carlo experiment modes are conducted, in which only a single uncertainty source is perturbed at a time while all others are held fixed at their baseline values. Each experiment mode consists of 1000 Monte Carlo realizations. For the single-source experiment modes, the coefficient of variation (CV) is computed to facilitate a comparative assessment of the relative importance of individual uncertainty sources.

3. Results

3.1. Emission model inputs statistics

This section summarizes the key input characteristics under the baseline setting. These baseline inputs form the reference scenario

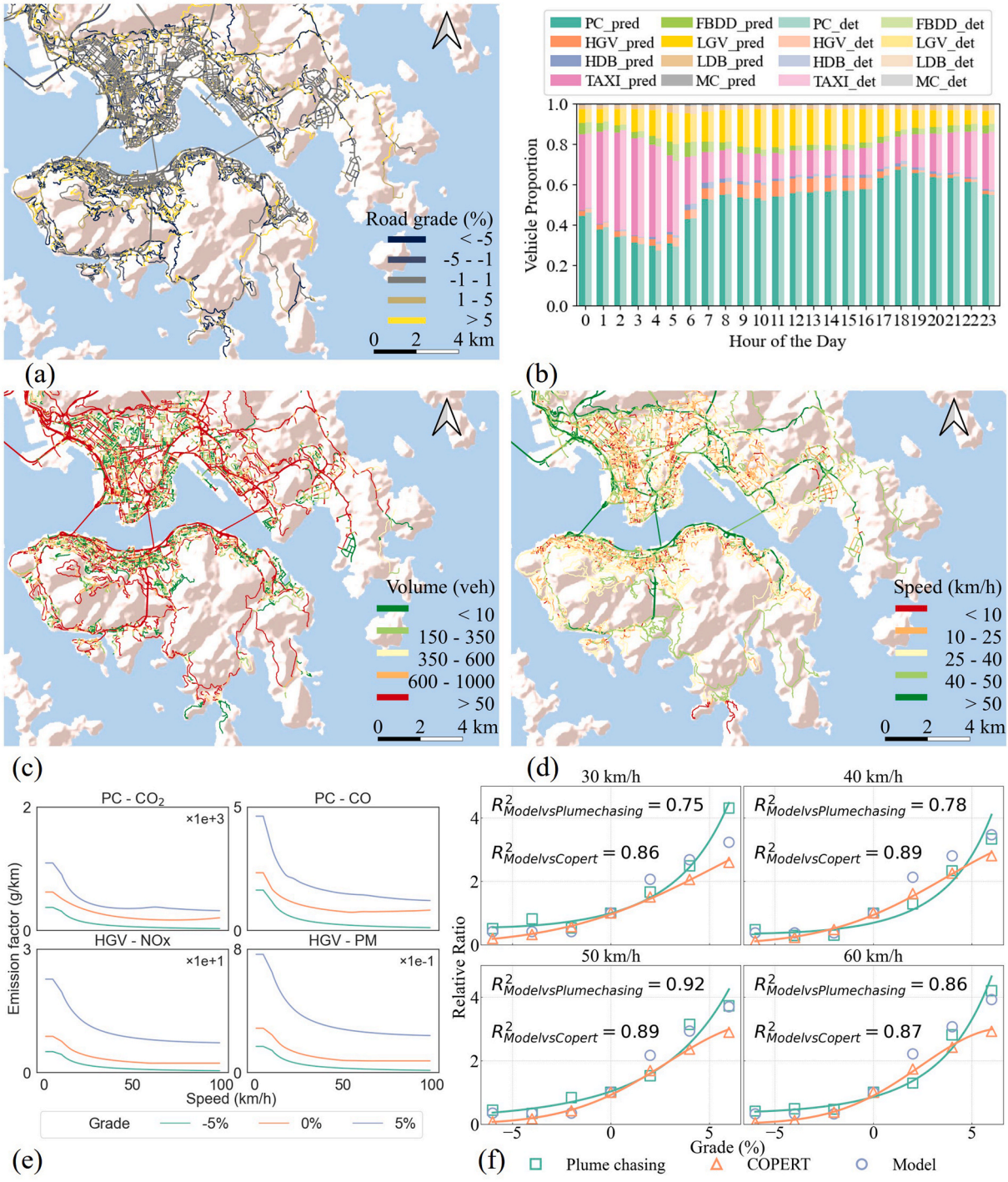

Fig. 2. (a) Link-level road grade in Hong Kong Island and Kowloon; (b) Hourly fleet composition on a specific weekday, where *vehicle class_pred* is derived from image-recognition results and *vehicle class_det* is derived from detector data; (c) Morning peak traffic volume map; (d) Morning peak traffic speed map; (e) Speed specific EFs for PC and HGV. Green, orange, and blue curves denote –5%, 0%, and 5% grades; (f) Comparison of relative ratio among on-road chasing measurement, COPERT, and model developed in this study for HGV. Fitted curves for relative ratios from on-road chasing measurement and COPERT across grades are in SI Table S6. (For interpretation of the references to colour in this figure legend, the reader is referred to the web version of this article.)

for all subsequent emission estimates.

3.1.1. Road grade estimation

Fig. 2(a) shows calculated road grades across Kowloon and Hong Kong Island, where the road grades for the whole HK road network are in the SI, section C5. To validate, the same method is applied to the HK 3D Pedestrian Network Map (HKLD, 2022), which provides sidewalk grade data. Comparing with the HK Pedestrian Network map, it shows that 96.54% of all road links have a grade difference of less than 5%. Considering the DTM data has up to 5-meter uncertainty, we believe the error is acceptable for our 100-meter road links. We observe 17.87% of road links have grades higher than 5%, indicating the hilly terrain in Hong Kong. In addition, assigning a zero grade to tunnels has a very limited impact on the city-scale emissions (SI, section C5).

3.1.2. Fleet composition

Baseline detection performance metrics of the computer vision model, reported prior to calibration, are provided in Fig. S11, ESI section C6. The city-scale hourly average fleet composition on a typical weekday is shown in Fig. 2(b), while fleet compositions for different days are provided in the ESI (Fig. S12, ESI section C6). The aggregated fleet composition estimated by the calibrated model closely matches that derived from detector data at both daily and hourly levels. Results indicate minimal variation across days but clear hourly fluctuations. For each of the 19 camera-detector pairs, hourly fleet compositions are computed from July 18, 2024, to August 10, 2024. RMSE and MAE are then calculated for each vehicle class, with distributions presented in ESI (Fig. S13, ESI section C6). Among the eight vehicle classes, the maximum RMSE is below 0.47 (average < 0.30), and the maximum MAE below 0.18 (average $<$ 0.07). Both metrics remain at relatively low levels, indicating that the calibrated computer vision model accurately and reliably estimates fleet composition across the road network. After interpolating fleet compositions to the full road network, we also validate the results by computing the mean absolute error (MAE) for each vehicle class. Across the 100 repetitions, the largest average MAE among vehicle classes remains below 0.025 (Fig. S14, ESI section C6), indicating that the interpolation method is accurate and feasible for estimating fleet compositions at unobserved road links.

3.1.3. Traffic flow

Fig. 2(c) and 2(d) show link-level traffic volume and speed maps during the morning peak in Kowloon and Hong Kong Island. Inverse distance weighting interpolation method performs well for estimating link-level traffic volume and speed (SI, section C2). The corresponding maps for the entire HK road network and distributions of traffic volume and speed are provided in SI, section C7. Between 08:00 and 18:00, more roads carry 150–600 vehicles/hour. Differences between morning and evening peaks appear mainly in the < 150 and > 1000 vehicles/hour bins, while overall distributions remain similar. Traffic speeds are mostly 10–40 km/h, peaking at 25–40 km/h. Over 25% of speeds exceed 50 km/h, indicating a relatively high operating speed. Despite HK's high population density, low per capita vehicle ownership contributes to great network efficiency. Similar speed distributions across peak hours suggest limited variation in traffic conditions. The temporal inconsistency between fleet composition and traffic flow data introduces only a limited influence on city-scale emission estimates (Figs. S15 and S16, ESI section C6).

3.1.4. Calculation and validation of emission factors

For the eight vehicle classes defined in this study, speed-specific EFs under given speeds and road grades are derived using the developed quantification method. Fig. 2(e) shows EFs for 2 representative vehicle classes (PC and HGV) at grades of −5%, 0%, and 5%. At the same speed, higher grades increase EFs, while lower grades reduce them, but reductions under negative grades do not fully offset increases from the same level of positive grades. Fig. 2(f) also reveals that EF sensitivity to grade varies by vehicle class, with heavier vehicles more affected. For heavier vehicles, grade-induced increments in VSP form a larger share of total VSP, while higher VSP yields greater ERs and thus higher EFs. Link-level EFs for all vehicle classes and pollutants across grades from −10% to 10% are in SI, section C8.

The grade-included EFs are validated through both plume chasing measurements in HK, literature, and the COPERT model. Specifically, we calculate EFs under different speed and grade conditions based on real-world plume chasing data, literature results, and the COPERT model. Absolute and relative residuals, relative ratios and $R^2_{\text{model vs. test}}$ (as defined in Section 2.5) are then derived to evaluate the consistency between the proposed grade-included EF model and the reference data sources (details in SI, section C9).

Results indicate that our model exhibits strong agreement with all reference datasets. In the validation based on on-road chasing measurement, all $R^2_{\text{model vs. test}}$ values exceed 0.75, demonstrating strong agreement between the model and field observations in HK. In the validation based on literature and COPERT model, all $R^2_{\text{model vs. test}}$ values exceed 0.5, and 7 out of 11 are above 0.8. The analysis results support the credibility of the developed model, demonstrating that it produces reliable estimates of grade-induced variations in emissions.

3.2. Comparison between emission estimates with and without road grade

Unless otherwise stated, all emission estimates reported in this section are based on baseline inputs, with uncertainty effects quantified separately using Monte Carlo simulations.

We first validate our modeling approach against the EMFAC-HK's burden mode, which is used in HK's regulatory framework to calculate area-specific emissions and report total emissions in tons per weekday. When not considering road grade effects, the estimated emission differences in 2019 are 1.90% for CO_2, 4.82% for CO, 1.12% for NO_X, and 1.43% for $PM_{2.5}$. The minor differences have demonstrated our model's validity, while showing that spatio-temporally resolved fleet composition does not significantly contribute

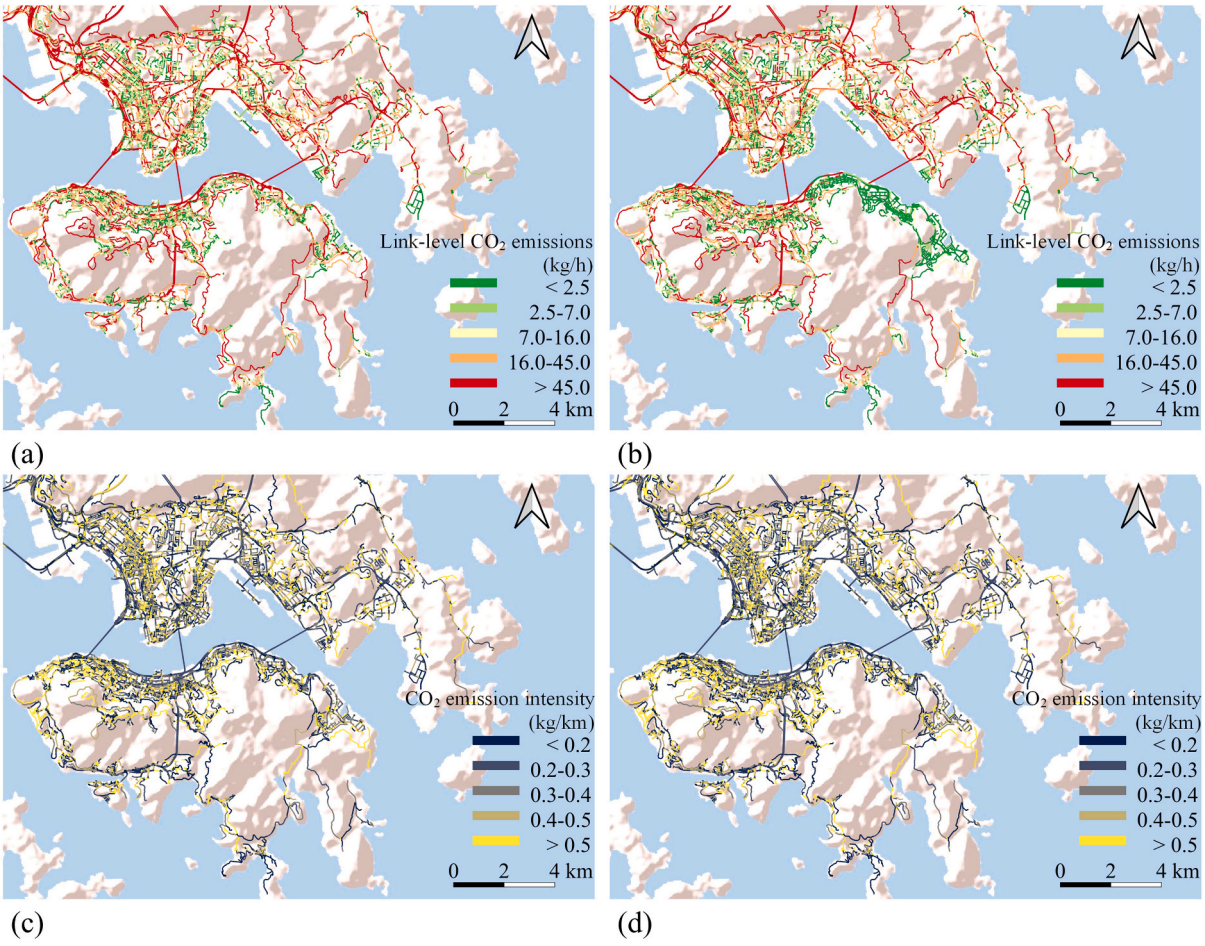

Fig. 3. Link-level CO_2 emissions in Hong Kong Island and Kowloon (a) CO_2 emissions per link during the morning peak hour (kg/h); (b) CO_2 emissions per link during the evening peak hour (kg/h). Emissions are classified into five ranges: <2.5, 2.5–7.0, 7.0–16.0, 16.0–45.0, and > 45.0 kg/h. (c) CO_2 emission intensity per VKT during the morning peak hour (kg/km); (d) CO_2 emission intensity per VKT during the evening peak hour (kg/km). Emission intensity is classified into five ranges: <0.2, 0.2–0.3, 0.3–0.4, 0.4–0.5, and > 0.5 kg/km.

to city-scale emission estimation uncertainty. We further examine the impact of neglecting vehicle acceleration on city-scale emission estimates and find that its influence is very limited (Fig. S33, ESI section C9). Fig. 3(a) and 3(b) present baseline link-level CO_2 emissions in Kowloon and Hong Kong Island during peak hours of 08:00–09:00 and 18:00–19:00, with the consideration of road grade. Emission calculations are conducted for each road link, as defined during the road grade computation, to capture grade effects on emissions accurately. During the morning peak, CO_2 emissions are approximately 1281.76 tons, versus 960.02 tons in the evening. Without considering road grade, CO_2 emissions during the morning and evening peaks are 1137.12 tons and 887.78 tons, respectively, indicating respective increases of 12.72% and 8.14% when grade is included. Entire road network emission maps for CO_2, CO, $PM_{2.5}$, and NO_X are provided in Fig. S36 and S37, ESI section C11. Incorporating road grade into the calculations leads to increases of 10.20%, 21.84%, and 17.83% for CO, $PM_{2.5}$, and NOx during the morning peak, and 8.55%, 15.99%, and 12.97% during the evening peak.

Fig. 3(c) and 3(d) illustrate CO_2 emissions normalized by VKT, representing emission intensity per distance. The spatial patterns closely resemble the road grade distribution in Fig. 2(a), underscoring topographic influence. Several segments—particularly those near the University of Hong Kong, Hong Kong Zoological and Botanical Gardens, and around the Happy Valley area in Hong Kong Island—show low total emissions but high per-VKT intensity, indicating that road grade significantly amplifies emissions even under comparable traffic conditions.

Under the baseline setting using mean operating conditions, the contributions of vehicle classes to emissions vary across pollutants and time periods, as shown in Fig. 4(a). For CO_2, the main contributors are PC, LGV, and HGV. CO emissions are primarily from PC, TAXI, and LDB, while LGV, HGV, and FBDD dominate NO_X and $PM_{2.5}$ emissions. Notably, TAXI is powered by liquefied petroleum gas, resulting in zero $PM_{2.5}$ emissions.

Within this baseline framework, road grade has a clear impact on city-scale emissions for most vehicle classes, especially HGV, FBDD, and LGV. For example, HGV CO_2 emissions increase from around 180 tons to over 250 tons during the morning peak, indicating that heavier vehicles are more sensitive to road grade. Similar trends are observed for LGV and FBDD across all pollutants. There are

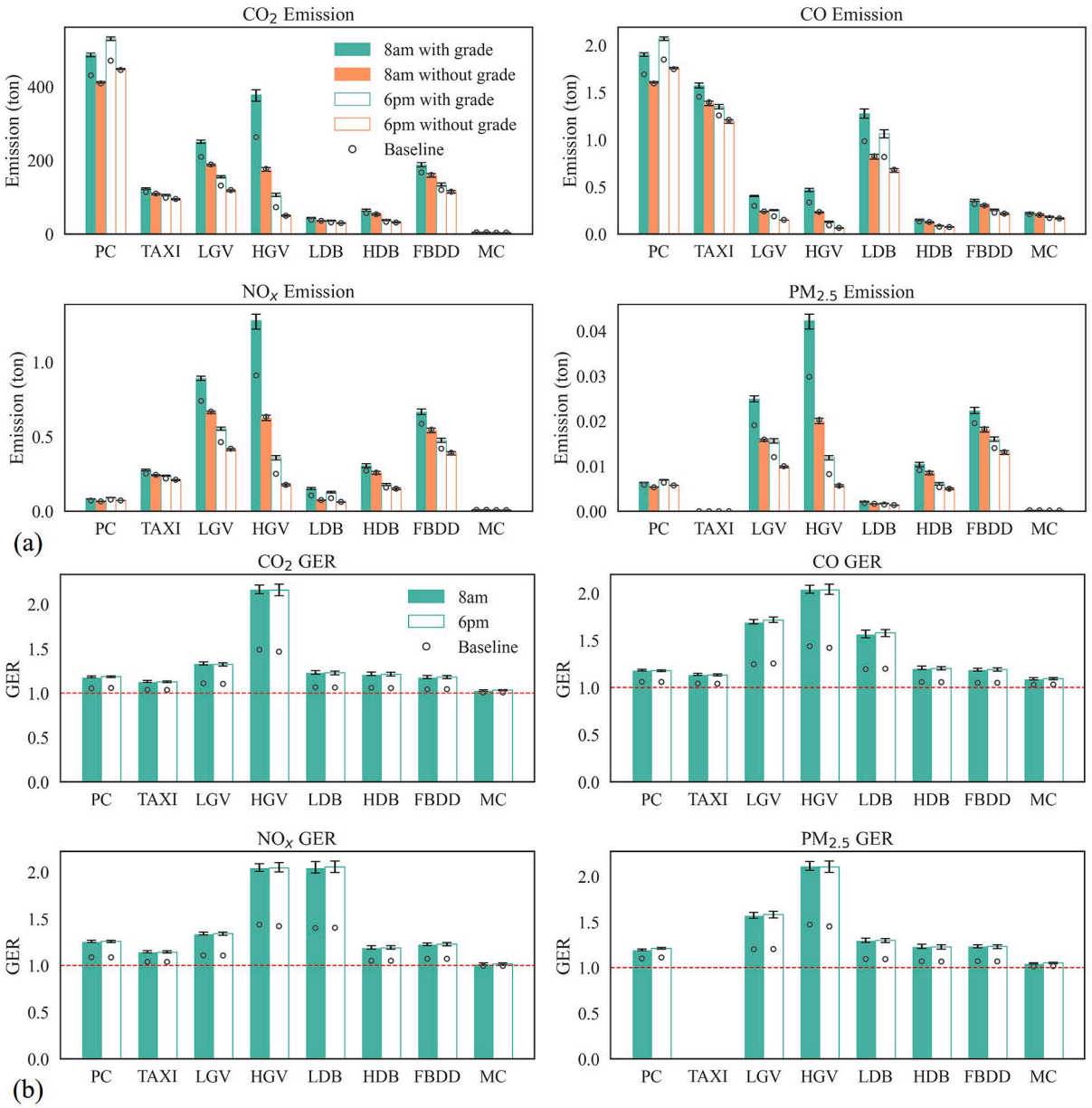

Fig. 4. (a) City-scale emissions of different vehicle classes with and without considering road grade during the morning and evening peak hours. Solid circles denote baseline estimates. Bars represent mean values from Monte Carlo simulations, and error bars indicate the corresponding 95% confidence intervals. (b) Grade Effect Ratios (GER), defined as the ratio of city-scale emissions calculated with and without considering road grade, by vehicle classes and pollutant. Solid circles denote baseline GER values, while bars and error bars represent Monte Carlo mean GER values and their 95% confidence intervals. The red dashed line indicates GER = 1. (For interpretation of the references to colour in this figure legend, the reader is referred to the web version of this article.)

also notable differences between morning and evening emissions. Both HGV and LGV exhibit significantly higher emissions during the morning peak. For instance, HGV emits nearly 0.9 tons of NO_X during the morning peak, compared to around 0.3 tons in the evening.

Fig. 4(a) also contrasts baseline estimates with Monte Carlo simulation results. Across most vehicle classes and pollutants, Monte Carlo mean values are consistently higher than the corresponding baseline estimates. This upward shift reflects the asymmetric emission response to road-grade variability, with comparable grade increases leading to larger emission increments than the emission reductions resulting from equivalent grade decreases. The confidence intervals obtained under the “with grade” and “without grade” cases are of comparable magnitude. This indicates that fluctuations in road grade contribute relatively little to the overall uncertainty range, whereas uncertainties associated with EFs, fleet composition, and traffic flow play a more dominant role in determining the width of the confidence intervals.

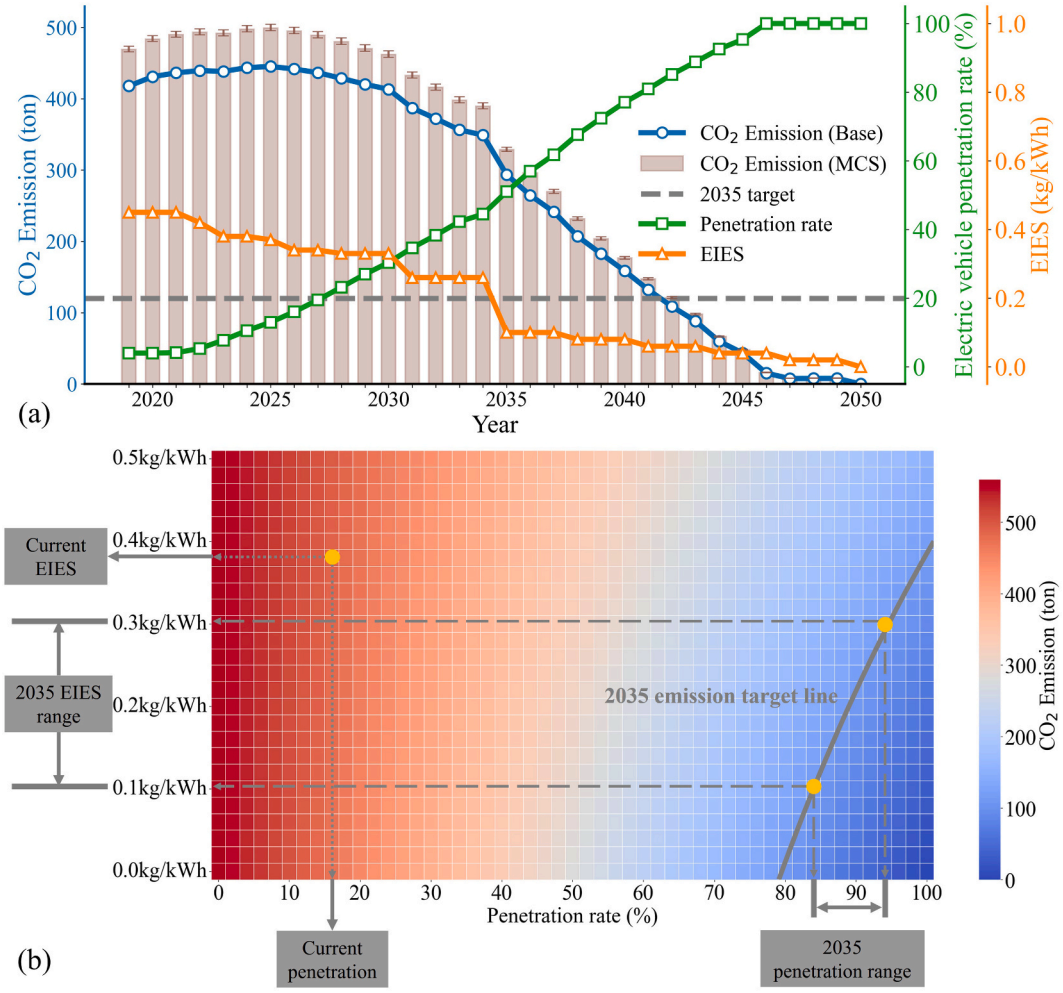

Fig. 5. (a) CO_2 emissions from PC during 2019–2050 under the current policy trajectory, considering the projected evolution of EV penetration and the EIES. The solid blue line denotes baseline emission estimates, while the bars and error bars represent the mean values of Monte Carlo simulation (MCS) and corresponding 95% confidence intervals. The horizontal dashed line indicates the 2035 emission reduction target. (b) CO_2 emissions from PC in 2035 under varying combinations of EIES and EV penetration rates. Results in panel (b) are calculated based on baseline estimates. (For interpretation of the references to colour in this figure legend, the reader is referred to the web version of this article.)

We define a Grade Effect Ratio (GER) as the ratio of city-scale emissions with and without road grade. Based on the baseline estimates (Fig. 4(b), points), GER values already exceed unity for all vehicle classes and pollutants, indicating that road grade leads to a net increase in emissions at the city scale. HGV and LGV are the main contributors and most grade-sensitive. For CO_2, the GER of HGV reaches approximately 1.49 during the morning peak and 1.47 during the evening peak, while LGV maintains a GER above 1.20 in both periods. For CO, both HGV and LGV exhibit GERs exceeding 1.42. For NO_X, HGV, and LDB show notable sensitivity, with GERs approaching 1.42 and 1.38, respectively. For $PM_{2.5}$, the GERs for HGV and LGV exceed 1.45 and 1.36, respectively.

Monte Carlo simulations further increase GER values across most vehicle classes and pollutants, as reflected by the bars in Fig. 4(b). For HGV, the Monte Carlo mean GER approaches or exceeds 2 under certain pollutants and time periods, indicating that uncertainty in road grade can nearly double the net emission effect relative to the no-grade case. This systematic increase in GER is consistent with the upward shift of Monte Carlo mean emission estimates observed in Fig. 4(a), confirming that uncertainty in road grade amplifies the emission effect of grade.

These indicate that vehicles are strongly affected by grades. While heavier vehicles are more grade-sensitive, GERs above 1.0 occur for all types, indicating grade effects are widespread. Importantly, all GERs > 1.0 show that downhill reductions cannot offset uphill increases, underscoring the cumulative burden of positive grades on network emissions.

3.3. *Decarbonization potential under integrated power-transport scenarios*

To halve CO_2 emissions by 2035 relative to 2005 and achieve carbon neutrality by 2050, HK has set strategic targets in both the

Table 1
City-scale emission uncertainty induced by different input sources.

Source	Pollutant	Mean (tons) (with/ without grade)	CV (%) (with/ without grade)
All sources	CO_2	1536.40/1133.04	0.49/0.25
	CO	6.35/4.90	0.46/0.34
	$PM_{2.5}$	0.11/0.07	0.88/0.61
	NO_X	3.66/2.48	0.72/0.47
Road grade derived from DTM data	CO_2	1543.73/1137.12	0.26/0.00
	CO	6.38/4.92	0.21/0.00
	$PM_{2.5}$	0.11/0.07	0.32/0.00
	NO_X	3.70/2.50	0.29/0.00
EFs associated with vehicle class aggregation	CO_2	1281.75/1137.12	0.10/0.05
	CO	5.42/4.92	0.08/0.04
	$PM_{2.5}$	0.09/0.07	0.32/0.16
	NO_X	2.94/2.50	0.09/0.08
Fleet composition estimation	CO_2	1276.18/1133.08	0.30/0.20
	CO	5.40/4.90	0.39/0.29
	$PM_{2.5}$	0.08/0.07	0.60/0.48
	NO_X	2.92/2.48	0.51/0.38
Fleet composition interpolation	CO_2	1278.86/1134.92	0.19/0.13
	CO	5.41/4.91	0.29/0.21
	$PM_{2.5}$	0.08/0.07	0.38/0.33
	NO_X	2.93/2.49	0.32/0.26
Traffic flow derived from the BDTMs	CO_2	1281.80/1137.10	0.03/0.02
	CO	5.42/4.92	0.03/0.02
	$PM_{2.5}$	0.09/0.07	0.04/0.03
	NO_X	2.94/2.50	0.03/0.03

transportation and energy sectors. Specifically, the government plans to cease registration of new non-electric PC by 2035 (HKEPD, 2021b). In parallel, major energy providers have committed to reducing the CO_2 emissions intensity of electricity sold (EIES, current 0.38 kg/kWh), with targets of 0.3 kg/kWh by 2030 and 0.1 kg/kWh by 2040 (CLP Group, 2024, 2021). This study evaluates city-scale CO_2 emissions from PC under various EIES and EV penetration scenarios, explicitly accounting for road grade, providing insights into coordinated low-carbon development pathways across the two sectors, with the morning peak hour as the primary illustration.

Fig. 5(a) illustrates city-scale CO_2 emissions from PC under the current policy projection. Estimated CO_2 emissions for EVs are expected to be conservative, as energy recovery from regenerative braking is not explicitly accounted for. As defined in Section 2.6, this trajectory reflects low-carbon electricity, EV uptake, and rising PC ownership under stable TDM conditions in HK. Under this trajectory, halving PC-related CO_2 emissions would likely occur only in the early 2040 s. Fig. 5(a) also contrasts the baseline trajectory with Monte Carlo results. Consistent with Fig. 4, Monte Carlo mean emissions are systematically higher than the corresponding baseline estimates.

Fig. 5(b) illustrates estimated city-scale CO_2 emissions from PC under various EV penetration rates and EIES, taking 2035 as an example. The gray curve represents the 2035 emission reduction target for PC (set at half of the 2005 level, i.e., 120 tons). Achieving the target requires an EV penetration of 84–94% and only if EIES falls to 0.1–0.3 kg/kWh. However, under the current policy trajectory, the EV penetration rate is projected to be only about 50% in 2035, and reaching a level above 84% would not occur until 2042, indicating the difficulty to rely solely on EV to achieve HK's transportation decarbonization goals on time.

The decarbonization scenarios examined in this study are designed in line with HK's official targets for new energy vehicle deployment and projected improvements in electricity carbon intensity. Future traffic activity in these scenarios is based on year-specific VKT from EMFAC-HK, which implicitly reflects expected long-term changes in travel demand (HKEPD, 2021a). The scenario analysis is intentionally focused on PC and the coupled evolution of PC electrification and power-sector decarbonization, for two reasons: EV penetration in Hong Kong remains low and accelerating PC electrification is a key near-term policy priority (HKEPD, 2025); and PCs are directly targeted by the planned phase-out of new non-electric PC registrations by 2035, making this segment particularly relevant for assessing progress toward the 2035 CO_2 reduction target (HKEPD, 2021b). Due to data availability and research scope constraints, this study does not explicitly model the energy use and upstream emissions of electric or hydrogen-powered heavy-duty vehicles, nor does it quantify modal shifts from PCs to public transport or active modes. Accordingly, the scenario design provides a tractable and quantifiable pathway for evaluating coordinated power–transport decarbonization at the city scale. Under this setting, the timing of emission reductions should be interpreted as illustrative outcomes under simplified assumptions, rather than precise forecasts of future system dynamics or behavioral feedback (e.g., congestion responses, rerouting, or induced demand).

Clearly, urban transport decarbonization requires a broader portfolio of strategies, including strengthened TDM, further shifts

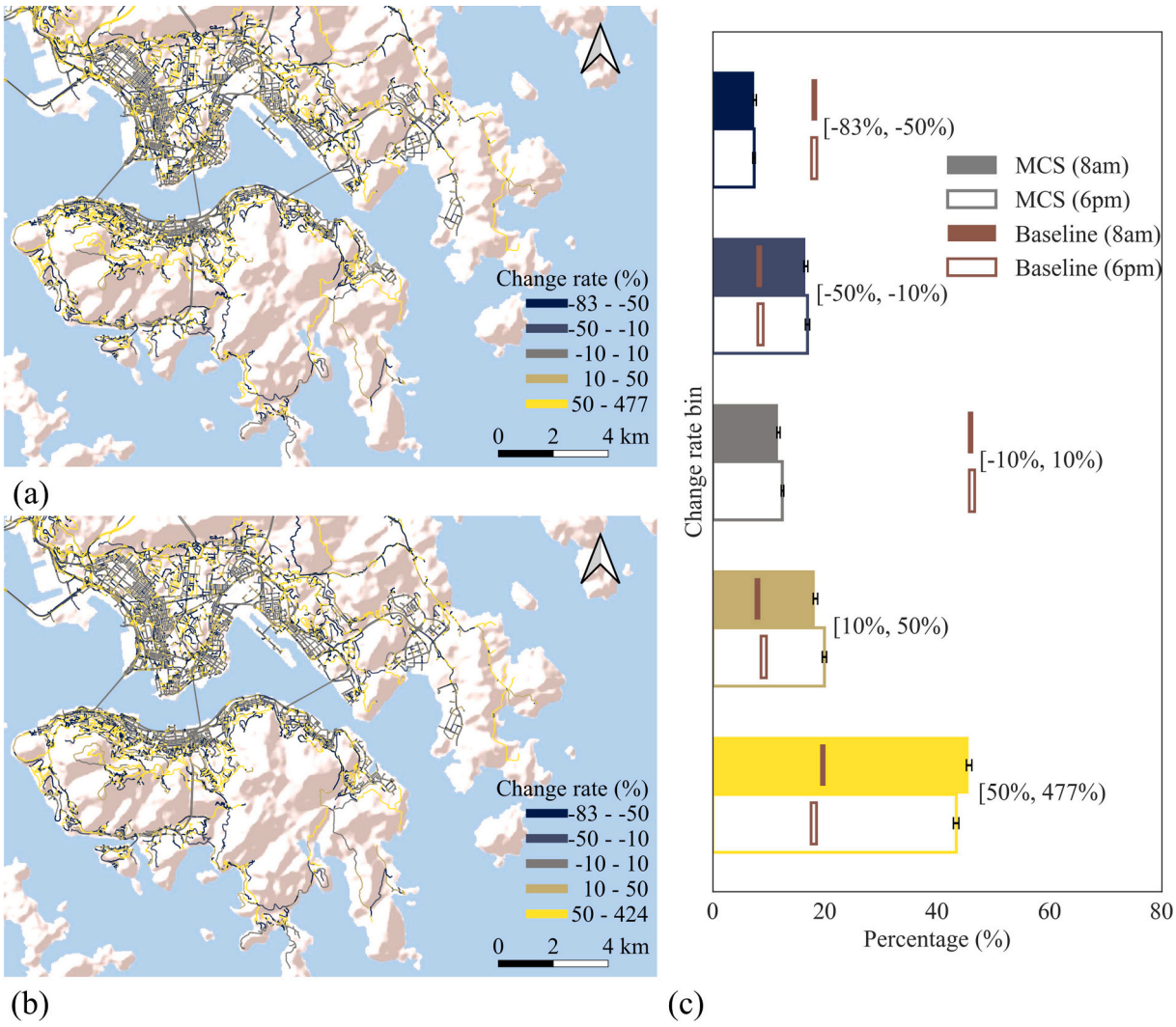

Fig. 6. A Change rates during the morning peak; (b) Change rates during the evening peak. Both calculated based on baseline estimates. Change rate is the proportional increase in NO_X emissions per link when road grade is considered, relative to no grade baseline. Change rates are classified into five ranges: −83% to −50%, −50% to −10%, −10% to 10%, 10% to 50%, and > 50% (up to 477% in the morning and 424% in the evening). (c) Distribution of road links across change-rate bins for the morning and evening peak hours. Solid bars represent distributions derived from Monte Carlo simulations (MCS), while outlined bars denote distributions based on baseline estimates.

toward public and active transport, and the decarbonization of freight fleets (Batur and Koç, 2017; Carroll et al., 2019; Mulholland et al., 2018). However, the additional mitigation potential of large-scale mode shift may be constrained in HK's local context, given its already high transit dependency (with over 90% of passenger trips completed by public transport), dense built environment, mountainous terrain, and limited road space (HKTD, 2025). In this context, our finding that ambitious EV penetration alone may be insufficient under carbon-intensive electricity supply highlights the central role of a clean electricity grid as a prerequisite for achieving substantial CO_2 reductions from vehicle electrification. Although integrated pathways are not explicitly quantified in this study, the proposed emission framework provides a foundation for future analyses that incorporate demand-side interventions, multimodal transitions, and cleaner freight technologies (e.g., battery-electric and hydrogen options), as well as other locally relevant measures such as improved traffic management and the decarbonization of water transport.

3.4. Uncertainty analysis

Table 1 summarizes the resulting mean emissions and coefficients of variation (CV) for the morning peak hour (results for the evening peak hour are reported in SI Section C12). Overall, the propagated uncertainty remains limited across all pollutants, with CV values below 1% in the joint uncertainty mode, indicating that the proposed emission framework is relatively robust to plausible variations in key input data.

Road grade uncertainty derived from DTM data exhibits relatively small CV values (typically below 0.3%). However, it leads to a noticeable increase in mean emissions when road grade is considered. This reflects the nonlinear response of emissions to road grade, whereby comparable grade increases lead to larger emission increments than the emission reductions resulting from equivalent grade decreases. It should be noted that this represents a conservative scenario, as real-world fluctuations in effective road grade are unlikely to approach the assumed ± 5% range.

Uncertainty associated with fleet composition shows a more pronounced effect on emission variability than road-grade or traffic-flow uncertainty, particularly for NO_X and $PM_{2.5}$. This is attributable to the disproportionate contribution of heavy-duty vehicles to these pollutants: changes in the relative share of heavy vehicles lead to larger absolute emission changes than comparable proportional variations in light-duty vehicles. In contrast, uncertainty in traffic flow derived from the BDTMs contributes negligibly to overall variability, with CV values consistently below 0.05% for all pollutants. These results indicate that while the overall uncertainty in city-scale emission estimates is modest, different uncertainty sources affect emission estimates through distinct mechanisms: vehicle class aggregation, fleet composition, and traffic flow mainly influence variability, whereas road-grade uncertainty induces systematic shifts in mean emission levels. This asymmetry arises from the nonlinear grade-emission relationship, such that positive grade perturbations increase emissions more strongly than equivalent negative perturbations reduce them, leading to an upward shift in the Monte Carlo mean.

4. Discussion

The emission differences before and after incorporating road grades are apparent and significant. In addition, we argue that the spatial distribution of emission hotspots can vary a lot given the dynamic nature of urban traffic, which has a fundamental impact on local low-emission traffic management and air quality control. We use NO_X emissions to illustrate the difference, which is considered a typical traffic-related air pollution, which are highly photochemically active with complex spatial–temporal distribution. NO_X emissions distributions during morning and evening peaks, under both scenarios—with and without road grade—are shown in Fig. S38, ESI section C11. Defining hotspots as links with NO_X emissions exceeding the 90th percentile of link-level NO_X emissions during each peak without considering road grade—150 g in the morning peak and 90 g in the evening peak—the number of hotspots increases by 18.7% in the morning peak (from 3306 to 3924) and 14.8% in the evening peak (from 3306 to 3795) after incorporating road grade. Meanwhile, 15.7% (519/3306) and 15.6% (515/3306) of morning and evening hotspots are re-categorized as non-hotspots, while another 34.3% and 30.4% previous non-hotspots are now hotspots, which denotes that incorporating road grade can lead to substantial changes in the spatial pattern of traffic emissions.

It is important to note that the hotspot analysis presented above is conducted under baseline conditions, using emission estimates derived from the original input data without stochastic perturbation. This baseline-based spatial comparison is intended to isolate the structural effect of road grade on the redistribution of emission hotspots.

Road grade effects intensify localized emissions, with additional hotspots concentrated in topographically complex areas such as Hong Kong Island, Kowloon, and Tsing Yi, where steep roads and heavy-duty traffic are common. These spatial shifts highlight the sensitivity of high-emission zones to terrain. NO_X emissions are mainly produced by heavy-duty diesel vehicles. As a result, residents in areas with high heavy-duty traffic flows, near logistics hubs, or along steep roads are more likely to face greater exposure to traffic-related air pollutants.

We define change rate as the proportional increase in NO_X emissions per road from the inclusion of road grade, relative to the baseline without grade consideration. The change rates in morning and evening peak hours are shown in Fig. 6 (a) and 6 (b), respectively. The most significant changes occur in Hong Kong Island, Kowloon, and Tsing Yi—areas with steep road segments and high traffic volumes—confirming substantial grade-induced increases in NOx emissions.

The distribution of links by change rate is shown in Fig. 6(c). About 46.7% of links fall within [-10%, 10%) in the morning peak, and 47.0% in the evening peak. In both periods, over half the links exhibit changes above ± 10% due to road grade, confirming the strong influence of topography. The maximum reduction is approximately 80%, while the maximum increase reaches 480%, underscoring significant uphill emission increases at the local level.

It should be noted that the spatial change-rate maps in Fig. 6(a) and 6(b) are based on the baseline. While Monte Carlo perturbations are applied to quantify uncertainty propagation, directly mapping Monte Carlo-averaged change rates would obscure the physical interpretation of terrain-induced emission hotspots, due to the highly nonlinear response of NOx emissions to road grade and the random nature of DTM perturbations. Therefore, the spatial maps are intended to illustrate the physical sensitivity of emissions to road grade under baseline conditions, whereas uncertainty effects are quantitatively summarized in Fig. 6(c) using Monte Carlo mean values and confidence intervals. The Monte Carlo results further indicate a pronounced shift in the distribution of change rates toward larger values, with a substantially higher proportion of links falling into the $\geq$ 50% change rate bin compared to the baseline. This behavior is again attributable to the asymmetric and nonlinear propagation of road grade uncertainty, whereby emission means are more sensitive to the increments induced by larger uphill grade compared to decrements from downhill.

The emission estimates obtained for HK are compared with city-scale road transport emission inventories reported for major metropolitan areas in North America and Europe (Table 2). These inventories are developed using established bottom-up models, including EMFAC, MOVES, and COPERT. Despite differences in base year, spatial scope, vehicle coverage, and EF formulations, the reported magnitudes of CO_2, CO, $PM_{2.5}$, and NO_X emissions are broadly comparable across cities. The HK estimates fall within the range reported for other large metropolitan areas, providing an order-of-magnitude benchmark and supporting the external consistency of the results.

In this study, multi-source open data—including traffic flow, emission factors (EFs), digital elevation model, road network maps,

Table 2
Comparison of city-scale road transport emission inventories for major metropolitan areas.

Research city	Population (million)	EFs model	Base year	Criteria Pollutant (tons/day)			
				CO_2	CO	$PM_{2.5}$	NO_X
Hong Kong (this study)	7.5	EMFAC-HK	2019	15679.4	76.7	1.3	41.0
Chong Qing (Duan et al., 2021)	32	LEAP-CQRT	2017	70137.0			
San Francisco Bay Area (BAAQMD, 2024)	7.5	EMFAC	2015		386.9	5.1	99.5
Greater Chicago Region (Lang et al., 2025)	9.5	MOVES	2017–2018			3.3–5.5	87.4–158.9
Greater Dublin Area* (Dey et al., 2019)	2.1	COPERT	2015	8027.4	61.3	0.9	19.0

*Only for passenger car.

and camera images—are integrated to conduct high-resolution, link-level road traffic emission estimation for Hong Kong. The impacts of road grade on city-scale traffic emissions and the spatial distribution of emission hotspots are apparent and necessary to include for mountainous cities. In addition, we conduct an analysis of the carbon reduction benefits of private car electrification under different electricity generation EFs. It is found that achieving a 50% reduction in CO_2 emissions from private cars by 2035 relative to 2005 levels is challenged by insufficient EV penetration rate and high EIES, with an about 7-year delay. The proposed framework provides a high-resolution paradigm for constructing city-scale traffic emission inventories using multi-source data, complemented by a detailed uncertainty analysis. While this study focuses on Hong Kong, the framework is transferable to other hilly cities, provided that key local inputs—such as fleet composition, EFs, traffic activity, and geographic information—are appropriately updated to reflect local conditions. In particular, transferring the framework to other cities would require recalibration of EFs to local fuel composition and emission factors, reconstruction of fleet composition to reflect key characteristics such as public transport shares and the proportions of different powertrain types (e.g., diesel and electric vehicles), and adaptation of road network characteristics and grade distributions. As these parameters are highly city-specific and depend on local data availability, this study does not conduct cross-city sensitivity analyses. Instead, the framework is intended to provide a structured methodology that can be re-implemented with locally appropriate inputs rather than a directly transferable set of results.

Future research will focus on improving the computer vision model to enhance recognition accuracy and enable reliable identification of electric vehicles. It will also calibrate BDTM-based traffic activity inputs using recent observations (e.g., camera-based counts or cordon counts), even though the 2019 BDTMs are the latest publicly released dataset available for Hong Kong, as travel demand may have changed in recent years, particularly following the COVID-19 pandemic. In addition, the VSP-related parameters currently adopted from the MOVES default settings will be calibrated using local data to better reflect Hong Kong–specific driving characteristics. Finally, data from additional cities will be collected to enable cross-city comparisons of how road grade affects pollutants and carbon emissions.

CRediT authorship contribution statement

Zeyu Zhang: Writing – review & editing, Writing – original draft, Validation, Methodology, Data curation, Conceptualization. **Qiuzi Chen:** Software, Data curation. **Weizhen Lin:** Software, Data curation. **Ran Tu:** Writing – review & editing, Methodology. **Wenyu Wang:** Methodology, Data curation. **Xiaotong Zhang:** Methodology, Data curation. **An Wang:** Writing – review & editing, Writing – original draft, Supervision, Conceptualization.

Declaration of competing interest

The authors declare that they have no known competing financial interests or personal relationships that could have appeared to influence the work reported in this paper.

Acknowledgement

This study is supported by the Young Scientists Fund of National Natural Science Foundation of China (Grant No.52500140). The authors would like to sincerely thank Prof. Zhen Leng and research assistant Weicheng Huang of the Hong Kong Polytechnic Univeristy for their valuable support in providing the vehicle for plume chasing experiments.

Appendix A. Supplementary data

Supplementary data to this article can be found online at https://doi.org/10.1016/j.trd.2026.105270.

Data availability

Data will be made available on request.

References

BAAQMD, 2024. Bay Area Emissions Inventory. Bay Area Air District.

Batur, İ., Koç, M., 2017. Travel demand management (TDM) case study for social behavioral change towards sustainable urban transportation in Istanbul. Cities 69, 20–35. https://doi.org/10.1016/j.cities.2017.05.017.

Bhujbal, A., Mane, D.T., 2020. Vehicle type classification using deep learning. In: Reddy, V.S., Prasad, V.K., Wang, J., Reddy, K.T.V. (Eds.), Soft Computing and Signal Processing. Springer Singapore, Singapore, pp. 279–290.

CARB, 2021. EMFAC2021 Volume I - User's Guide. Mobile Source Analysis Branch, Air Quality Planning & Science Division, California Air Resource Board, Sacramento, CA.

Carroll, P., Caulfield, B., Ahern, A., 2019. Measuring the potential emission reductions from a shift towards public transport. Transp. Res. Part D: Transp. Environ. 73, 338–351. https://doi.org/10.1016/j.trd.2019.07.010.

CLP Group, 2021. Helping Hong Kong achieve its decarbonisation goal [WWW Document]. URL https://sustainability.clpgroup.com/en/2021/case-studies (accessed 4.25.25).

CLP Group, 2024. Together for sustainability, power tomorrow - 2024 Sustainability Report.

Dey, S., Caulfield, B., Ghosh, B., 2019. Modelling uncertainty of vehicular emissions inventory: a case study of Ireland. J. Clean. Product. 213, 1115–1126. https://doi.org/10.1016/j.jclepro.2018.12.125.

Duan, L., Hu, W., Deng, D., Fang, W., Xiong, M., Lu, P., Li, Z., Zhai, C., 2021. Impacts of reducing air pollutants and CO2 emissions in urban road transport through 2035 in Chongqing, China. Environ. Sci. Ecotechnol. 8, 100125. https://doi.org/10.1016/j.ese.2021.100125.

Frey, H.C., Zhang, K., Rouphail, N.M., 2008. Fuel use and emissions comparisons for alternative routes, time of day, road grade, and vehicles based on in-use measurements. Environ. Sci. Technol. 42, 2483–2489. https://doi.org/10.1021/es702493v.

Friedrich, M., Pestel, E., Schiller, C., Simon, R., 2019. Scalable GEH: a quality measure for comparing observed and modeled single values in a travel demand model validation. Trans. Res. Rec. 2673, 722–732. https://doi.org/10.1177/0361198119838849.

Fu, X., Wu, P., 2025. Measurement methods and influencing factors of carbon emissions from residents' travel. Appl. Energy 377, 124733. https://doi.org/10.1016/j.apenergy.2024.124733.

He, L., You, Y., Zheng, X., Zhang, S., Li, Z., Zhang, Z., Wu, Y., Hao, J., 2022. The impacts from cold start and road grade on real-world emissions and fuel consumption of gasoline, diesel and hybrid-electric light-duty passenger vehicles. Sci. Total Environ. 851, 158045. https://doi.org/10.1016/j.scitotenv.2022.158045.

HKEPD, 2025. Promotion of Electric Vehicles | Environmental Protection Department [WWW Document]. URL https://www.epd.gov.hk/epd/english/environmentinhk/air/promotion_ev/promotion_ev.html (accessed 1.25.26).

HKTD, 2025. Transport Department - Introduction [WWW Document]. URL https://www.td.gov.hk/en/transport_in_hong_kong/its/introduction/index.html?utm_source=chatgpt.com (accessed 1.25.26).

HKEPD, 2021a. EMFAC-HK User's Guide Version 4.x: Calculating emission inventories for vehicles in Hong Kong. Hong Kong Environmental Protection Department.

HKEPD, 2021b. Hong Kong's Climate Action Plan 2050.

HKLD, 2019. Lands Department - Key features of DTM [WWW Document]. URL https://www.landsd.gov.hk/en/spatial-data/open-data/kf_dtm.html (accessed 4.9.25).

HKLD, 2022. 3D Pedestrian Network | DATA.GOV.HK [WWW Document]. URL https://data.gov.hk/en-data/dataset/hk-landsd-openmap-3d-pedestrian-network (accessed 4.13.25).

HKTD, 2021. Transport Department - The 2019 Base District Traffic Models [WWW Document]. URL https://www.td.gov.hk/en/publications_and_press_releases/publications/other_publications/bdtm/index.html (accessed 4.9.25).

Jimenez-Palacios, J.L., 1998. Understanding and quantifying motor vehicle emissions with vehicle specific power and TILDAS remote sensing. Citeseer.

Kumar, H., Mamoria, P., Dewangan, D.K., 2025. Improving Faster R-CNN for Vehicle Detection under Varying Conditions with Domain Adaptation Technique, in: 2025 Fourth International Conference on Power, Control and Computing Technologies (ICPC2T). Presented at the 2025 Fourth International Conference on Power, Control and Computing Technologies (ICPC2T), IEEE, Raipur, India, pp. 1–6. DOI: 10.1109/ICPC2T63847.2025.10958674.

Kumar, A., Kashiyama, T., Maeda, H., Omata, H., Sekimoto, Y., 2022. Real-time citywide reconstruction of traffic flow from moving cameras on lightweight edge devices. ISPRS J. Photogramm. Remote Sens. 192, 115–129.

Lang, V.A., Camilleri, S.F., Van Der Lee, S., Rowangould, G., Antonczak, B., Thompson, T.M., Harris, M.H., Harkins, C., Tong, D.Q., Janssen, M., Adelman, Z.E., Horton, D.E., 2025. Intercomparison of modeled urban-scale vehicle NO_x and $PM_{2.5}$ emissions–implications for equity assessments. Environ. Sci. Technol. 59, 4560–4570. https://doi.org/10.1021/acs.est.4c09777.

Lejri, D., Leclercq, L., 2020. Are average speed emission functions scale-free? Atmos. Environ. 224, 117324. https://doi.org/10.1016/j.atmosenv.2020.117324.

Li, Y., Lv, C., Yang, N., Liu, H., Liu, Z., 2020. A study of high temporal-spatial resolution greenhouse gas emissions inventory for on-road vehicles based on traffic speed-flow model: a case of Beijing. J. Clean. Product. 277, 122419. https://doi.org/10.1016/j.jclepro.2020.122419.

Li, H., Wen, Y., Wu, R., Wang, Y., Zhou, Z., Deng, Y., Tan, Q., Xiao, L., Wu, X., Zhang, S., Wu, Y., 2024. Assessing traffic emissions during the summer world university games 2023: Insights for multisectoral synergetic decontamination. Sci. Total Environ. 954, 176488. https://doi.org/10.1016/j.scitotenv.2024.176488.

Liu, Y., Huang, W., Lin, X., Xu, R., Li, L., Ding, H., 2022. Variation of spatio-temporal distribution of on-road vehicle emissions based on real-time RFID data. J. Environ. Sci. 116, 151–162. https://doi.org/10.1016/j.jes.2021.07.018.

Liu, J., Li, J., Chen, Y., Lian, S., Zeng, J., Geng, M., Zheng, S., Dong, Y., He, Y., Huang, P., Zhao, Z., Yan, X., Hu, Q., Wang, L., Yang, D., Zhu, Z., Sun, Y., Shang, W., Wang, D., Zhang, L., Hu, S., Chen (Michael), X., 2023. Multi-scale urban passenger transportation CO2 emission calculation platform for smart mobility management. Appl. Energy 331, 120407. https://doi.org/10.1016/j.apenergy.2022.120407.

Liu, Y.-H., Ma, J.-L., Li, L., Lin, X.-F., Xu, W.-J., Ding, H., 2018. A high temporal-spatial vehicle emission inventory based on detailed hourly traffic data in a medium-sized city of China. Environ. Pollut. 236, 324–333. https://doi.org/10.1016/j.envpol.2018.01.068.

Ma, C., Xue, F., 2024. A review of vehicle detection methods based on computer vision. J. Intell. Connect. Vehicles 7, 1–18. https://doi.org/10.26599/JICV.2023.9210019.

Mera, Z., Varella, R., Baptista, P., Duarte, G., Rosero, F., 2022. Including engine data for energy and pollutants assessment into the vehicle specific power methodology. Appl. Energy 311, 118690. https://doi.org/10.1016/j.apenergy.2022.118690.

Morris, B.T., Tran, C., Scora, G., Trivedi, M.M., Barth, M.J., 2012. Real-time video-based traffic measurement and visualization system for energy/emissions. IEEE Trans. Intell. Trans. Syst. 13, 1667–1678.

Mulholland, E., Teter, J., Cazzola, P., McDonald, Z., Gallachóir, Ó.B.P., 2018. The long haul towards decarbonising road freight – a global assessment to 2050. Appl. Energy 216, 678–693. https://doi.org/10.1016/j.apenergy.2018.01.058.

Nekkanti, L.K.K., Rao, V., 2023. A Yolo-Based Deep Learning Approach for Vehicle Class Classification, in: Morusupalli, R., Dandibhotla, T.S., Atluri, V.V., Windridge, D., Lingras, P., Komati, V.R. (Eds.), Multi-Disciplinary Trends in Artificial Intelligence. Springer Nature Switzerland, Cham, pp. 554–568.

Ntziachristos, L., Gkatzoflias, D., Kouridis, C., Samaras, Z., 2009. COPERT: A European Road Transport Emission Inventory Model, in: Athanasiadis, I.N., Rizzoli, A.E., Mitkas, P.A., Gómez, J.M. (Eds.), Information Technologies in Environmental Engineering. Springer Berlin Heidelberg, Berlin, Heidelberg, pp. 491–504.

Ojha, A., Sahu, S.P., Dewangan, D.K., 2021. Vehicle Detection through Instance Segmentation using Mask R-CNN for Intelligent Vehicle System, in: 2021 5th International Conference on Intelligent Computing and Control Systems (ICICCS). Presented at the 2021 5th International Conference on Intelligent Computing and Control Systems (ICICCS), IEEE, Madurai, India, pp. 954–959. DOI: 10.1109/ICICCS51141.2021.9432374.

Papadopoulos, G., Ntziachristos, L., Tziourtzioumis, C., Keramydas, C., Lo, T.-S., Ng, K.-L., Wong, H.-L.-A., Wong, C.-K.-L., 2020. Real-world gaseous and particulate emissions from Euro IV to VI medium duty diesel trucks. Sci. Total Environ. 731, 139137. https://doi.org/10.1016/j.scitotenv.2020.139137.

Satyanarayana, G.S.R., Deshmukh, P., Das, S.K., 2022. Vehicle detection and classification with spatio-temporal information obtained from CNN. Displays 75, 102294. https://doi.org/10.1016/j.displa.2022.102294.

Suarez, J., Makridis, M., Anesiadou, A., Komnos, D., Ciuffo, B., Fontaras, G., 2022. Benchmarking the driver acceleration impact on vehicle energy consumption and CO2 emissions. Transport. Res. D: Trans. Environ. 107, 103282. https://doi.org/10.1016/j.trd.2022.103282.

U.S. EPA, 2023. Exhaust Emission Rates for Light-Duty Onroad Vehicles in MOVES4 (No. EPA-420-R-23-028). U.S. Environmental Protection Agency.

Wang, A., Tu, R., Gai, Y., Pereira, L.G., Vaughan, J., Posen, I.D., Miller, E.J., Hatzopoulou, M., 2020a. Capturing uncertainty in emission estimates related to vehicle electrification and implications for metropolitan greenhouse gas emission inventories. Appl. Energy 265, 114798. https://doi.org/10.1016/j.apenergy.2020.114798.

Wang, A., Xu, J., Tu, R., Saleh, M., Hatzopoulou, M., 2020b. Potential of machine learning for prediction of traffic related air pollution. Transport. Res. D: Trans. Environ. 88, 102599.

Wang, A., Xu, J., Zhang, M., Zhai, Z., Song, G., Hatzopoulou, M., 2022. Emissions and fuel consumption of a hybrid electric vehicle in real-world metropolitan traffic conditions. Appl. Energy 306, 118077. https://doi.org/10.1016/j.apenergy.2021.118077.

Wang, A., Weichenthal, S., Lloyd, M., Hong, K., Saxe, S., Hatzopoulou, M., 2023a. Personal mobility choices and disparities in carbon emissions. Environ. Sci. Technol. 57, 8548–8558. https://doi.org/10.1021/acs.est.2c06993.

Wang, H., Zhang, S., Wu, X., Wen, Y., Li, Z., Wu, Y., 2023b. Emission measurements on a large sample of heavy-duty diesel trucks in China by using mobile plume chasing. Environ. Sci. Technol. 57, 15153–15161. https://doi.org/10.1021/acs.est.3c03028.

Wen, Y., Zhang, S., Zhang, J., Bao, S., Wu, X., Yang, D., Wu, Y., 2020. Mapping dynamic road emissions for a megacity by using open-access traffic congestion index data. Appl. Energy 260, 114357. https://doi.org/10.1016/j.apenergy.2019.114357.

Wen, Y., Wu, R., Zhou, Z., Zhang, S., Yang, S., Wallington, T.J., Shen, W., Tan, Q., Deng, Y., Wu, Y., 2022. A data-driven method of traffic emissions mapping with land use random forest models. Appl. Energy 305, 117916. https://doi.org/10.1016/j.apenergy.2021.117916.

Wen, Y., Liu, M., Zhang, S., Wu, X., Wu, Y., Hao, J., 2023. Updating on-road vehicle emissions for china: spatial patterns, temporal trends, and mitigation drivers. Environ. Sci. Technol. 57, 14299–14309. https://doi.org/10.1021/acs.est.3c04909.

Wen, Y., Zhang, S., Wang, Y., Yang, J., He, L., Wu, Y., Hao, J., 2024. Dynamic traffic data in machine-learning air quality mapping improves environmental justice assessment. Environ. Sci. Technol. acs.est.3c07545. https://doi.org/10.1021/acs.est.3c07545.

WRI, 2022. Decarbonising Hong Kong's Roads: Pathways Towards a Net-Zero Road Transport System. World Resources Institute.

Wyatt, D.W., Li, H., Tate, J.E., 2014. The impact of road grade on carbon dioxide (CO2) emission of a passenger vehicle in real-world driving. Transport. Res. Part D: Trans. Environ. 32, 160–170. https://doi.org/10.1016/j.trd.2014.07.015.

Xiang, S., Zhang, S., Yu, Y.T., Wang, H., Shen, Y., Zhang, Q., Wang, Z., Wang, D., Tian, M., Wang, J., Yin, H., Jiang, J., Wu, Y., 2023. Evaluation of the relationship between meteorological variables and NO $_x$ emission factors based on plume-chasing measurements. ACS EST Eng. 3, 417–426. https://doi.org/10.1021/acsestengg.2c00317.

Xiang, S., Zhang, S., Yu, Y.T., Wang, H., Hao, K., Wu, Y., 2025. Significant NO_2 formation in truck exhaust plumes and its association with ambient O_3 : evidence from extensive plume-chasing measurement. Environ. Sci. Technol. 59, 4014–4024. https://doi.org/10.1021/acs.est.4c07804.

Yang, Y., Yang, Y., Zhang, B., Cheng, P., Lee, D.-H., Hu, S., 2024. Traffic Emission Estimation and Modelling at Urban Intersections Using High-Resolution UAV-Based Video. In: 2024 Forum for Innovative Sustainable Transportation Systems (FISTS). Presented at the 2024 Forum for Innovative Sustainable Transportation Systems (FISTS), pp. 1–6. https://doi.org/10.1109/FISTS60717.2024.10485600.

Yang, D., Zhang, S., Niu, T., Wang, Y., Xu, H., Zhang, K.M., Wu, Y., 2019. High-resolution mapping of vehicle emissions of atmospheric pollutants based on large-scale, real-world traffic datasets. Atmos. Chem. Phys. 19, 8831–8843. https://doi.org/10.5194/acp-19-8831-2019.

Zachiotis, A.T., Giakoumis, E.G., 2020. Methodology to estimate road grade effects on consumption and emissions from a light commercial vehicle running on the WLTC cycle. J. Energy Eng. 146, 04020048. https://doi.org/10.1061/(ASCE)EY.1943-7897.0000694.

Zhang, S., Wu, Y., Huang, R., Wang, J., Yan, H., Zheng, Y., Hao, J., 2016. High-resolution simulation of link-level vehicle emissions andconcentrations for air pollutants in a traffic-populated eastern asian city. Atmos. Chem. Phys. 16, 9965–9981. https://doi.org/10.5194/acp-16-9965-2016.

Zhang, S., Niu, T., Wu, Y., Zhang, K.M., Wallington, T.J., Xie, Q., Wu, X., Xu, H., 2018. Fine-grained vehicle emission management using intelligent transportation system data. Environ. Pollut. 241, 1027–1037. https://doi.org/10.1016/j.envpol.2018.06.016.